Evaluation of guaiacyl lignin aromatic structures using $^{13}CO_2$ administered *Ginkgo biloba* L. xylem by quantitative solid- and liquid-state ^{13}C NMR

Sonoka MIYATA[1], Dan AOKI[1*], Yasuyuki MATSUSHITA[2], Miyuki TAKEUCHI[3], Kazuhiko FUKUSHIMA[1]

[1] Graduate School of Bioagricultural Sciences, Nagoya University, Nagoya 464-8601, Japan

[2] Institute of Agriculture, Tokyo University of Agriculture and Technology, Tokyo 183-8509, Japan

[3] Institute of Engineering Innovation, School of Engineering, The University of Tokyo, Tokyo 113-8656, Japan

* Corresponding author: aoki.dan@nagoya-u.jp

Abstract

Ginkgo biloba L. saplings were cultivated in an airtight growth chamber with $^{13}CO_2$ for two months. The ^{13}C ratio of the newly developed xylem region was ca. 85%, evaluated by high lateral resolution secondary ion mass spectrometry and thioacidolysis/GC-MS. Quantitative solid-state ^{13}C direct polarisation/magic angle spinning (DP/MAS) NMR measurements with high-speed MAS of 70.0 kHz were conducted for cutting-milled wood (CMW), ball-milled wood (BMW), and enzymatically saccharified lignin (EL) samples. In addition, quantitative liquid-state ^{13}C NMR measurements were carried out for EL in DMSO-d_6. Major lignin aromatic signals were classified into three groups of aromatic carbons of C-H, C-C, and C-O, and their area ratio was compared within these measurements. EL samples in solid- and liquid-state showed nearly the same results. However, the results for CMW and BMW in solid-state NMR suggest the structural alteration of lignin within the sample preparation procedure, including ball milling.

Keywords:

13CO2, lignin, *Ginkgo biloba* L., solid-state NMR, quantitative NMR

Introduction

Lignin is one of the major plant cell wall components, which has a highly complicated structure formed by the radical coupling of monolignols. The general functions of lignin in plants are to give the stems rigidity, assist in water movement, and protect plants against biological attack (Niklas and Pratt 1980; Dimmel 2010). Despite various studies, the chemical structure of native lignin has not been completely understood. Elucidating lignin structure is essential to improve our

knowledge of its chemical and physical characteristics in the cell wall and convert woody biomass into valuable materials. Various methods, mainly chemical cleavage methods, have been developed to estimate the chemical structure of lignin (Tai et al. 1990; Lapierre et al. 1985, 1991, 1995; Lu and Ralph 1997). However, the structural information obtained by chemical cleavage methods is limited and not enough to describe the native lignin in the plant cell walls.

NMR spectroscopy has been applied to estimate the entire lignin structure for a long time. Mainly, solution-state NMR has been used for lignin structural analysis. Various types of interunit linkages in lignin have been qualitatively and quantitatively revealed by such as ^{1}H, ^{13}C, and ^{1}H-^{13}C HSQC NMR measurements (Nimz et al. 1981; Guittet et al. 1985; Landucci 1985; Xia et al. 2001; Lu and Ralph 2003; Capanema et al. 2004; Ralph et al. 2006, 2012; Nishimura et al. 2018). However, interunit linkages involved in aromatic guaiacyl ring-5 carbon are various, such as not condensed (C-H), condensed (C-C as β-5, 5-5, dibenzodioxocin), and etherified (C-O as 4-O-5) structures. The quaternary carbons limit the application of H-based multidimensional NMR techniques and quantitativity. Moreover, in lignin structural studies using solution-state NMR, lignin chemical structure can be altered during the pretreatment of ball-milling (Ikeda et al. 2002; Fujimoto et al. 2005; Guerra et al. 2006; Hu et al. 2006). As previous studies showed, ball-milling can induce cleavage of β-*O*-4 bonds and the formation of other bonds. On the other hand, there is a report suggesting that lignin was not significantly affected by ball milling (Sipponen et al. 2014). From these points, to elucidate the chemical structure of lignin in a natural state, it is essential to examine an appropriate preparation method and know how it alters the lignin structure.

Solid-state NMR is a promising way to elucidate the structural and physical properties of lignin in the natural state. The wood powder can be applied to solid-state NMR measurements directly. Structural, physical, and chemical characterisation of components in plant cell walls such as cellulose, hemicellulose, and lignin have been examined by solid-state NMR (Hatcher 1987; Lesage et al. 1999; Terashima et al. 2002; Wikberg and Maunu 2004; Mao et al. 2006). However, as previous studies show, the ^{13}C signals of lignin are broad in solid-state NMR and weak compared with other signals, such as cellulose and hemicellulose. Thus, it is also difficult to discuss the lignin structure quantitatively and in detail. Although solid-state NMR is a promising approach, little has been reported on the quantitative analysis of lignin in the whole cell wall.

In the previous study (Aoki et al. 2019), the authors obtained selectively ^{13}C labelled *Ginkgo biloba* L. lignin by administrating [guaiacyl ring-5-^{13}C]-coniferin to a growing *G. biloba* shoot, prepared the ^{13}C-enriched enzymatically saccharified lignin (EL) sample and examined solid- and liquid-state ^{13}C NMR spectroscopy to elucidate the ring-5 structure. As a result, peak area variations of resolved ring-5 derived signals depending on the contact time by solid-state ^{13}C cross polarisation/

magic angle spinning (CP/MAS) NMR suggest that the bonding patterns in lignin might affect their local molecular mobility. However, the solid-state ^{13}C CP/MAS NMR quantification using the contact time extrapolation method disagreed with the quantitative liquid-state NMR measurement result. Thus, the quantitative discussion of the native structure of lignin in plant cell walls needs higher sensitivity in solid-state NMR to use more quantitative solid-state ^{13}C direct polarisation (DP)/MAS NMR measurements. This method is also called dipolar decoupling (DD)/MAS.

In this study, to dramatically improve the sensitivity of lignin in NMR measurements, a ^{13}C-enriched sample was prepared by $^{13}CO_2$ administration to *Ginkgo biloba* L. saplings for two months. In order to estimate the ^{13}C ratio in the whole cell wall and lignin, a transverse section and wood powder were prepared and submitted to a high lateral resolution secondary ion mass spectroscopy (NanoSIMS) and thioacidolysis, respectively. Following the preparation of wood powder, minimum ball-milling, DMAc-LiCl dissolution and enzymatic saccharification process was employed to prepare the enzymatically saccharified lignin (EL) sample. Finally, cutting-milled wood (CMW), ball-milled wood (BMW), and EL samples were applied to quantitative NMR measurements. Furthermore, a high-speed MAS of 70.0 kHz was used for solid-state ^{13}C DP/MAS NMR measurements to operate peak fitting procedures better. The structural alteration of lignin in the sample preparation processes was discussed.

Materials and methods

Materials:

G. biloba saplings (500–600 mm in height) were purchased from Toyama Green Ltd. (Kumamoto, Japan) and cultivated in a room for 2 months before the experiments. Four young trees of *G. biloba* were placed into pots (150-mm diameter) and covered with rock wool (Grodan, ROCKWOOL B.V.). Synthesised air (Air Liquide Japan G.K., Tokyo, Japan), CO_2 (Nagoya Nissan Inc., Nagoya, Japan), and $^{13}CO_2$ (^{13}C : 99 %, Cambridge Isotope Laboratories, Inc., Tewksbury, US) were purchased and used as received. Other chemical reagents were purchased from Kishida Chemical Co., Ltd. (Osaka, Japan), Kanto Chemical Co., Inc. (Tokyo, Japan), FUJIFILM Wako Pure Chemical Corporation (Osaka, Japan), Tokyo Chemical Industry Co., Ltd. (Tokyo, Japan), or Merck KGaA (Darmstadt, Germany) and used as received.

Incubation of *G. biloba* saplings in a $^{13}CO_2$ atmosphere:

G. biloba saplings were cultivated in an airtight growth chamber (Fig. 1, a custom-made by SHINKOKASEI Inc., Gifu, Japan. External dimension 600×600×1000 mm^3, internal dimension 580×580×970 mm^3, 326 L in volume) equipped with a dehumidifier (TU-400, THREEUP Inc., Osaka,

Japan), data logger ($^{12}CO_2$ concentration, temperature, and relative humidity, TR-76Ui, T&D Corp., Matsumoto, Japan), USB fan, water-flow cooling pipe unit, and LED light (VEFA140WZG vegefarm, ALTRADER, Yokohama, Japan). In addition, the growth chamber has water, synthesised air, and CO_2 inlet valves. An overview and a photograph of the growth chamber, temperature and relative humidity in the chamber (recorded for every 15 min) are shown in Fig. S1 and S2, respectively.

The airtight ability and the average and apparent CO_2 assimilation rate were evaluated using the $^{12}CO_2$ concentration. After an air purge of the chamber, the CO_2 concentration was monitored, and the increment was 1.25 ppm/h without plant samples, which suggests its high airtight ability. The average and apparent CO_2 decrement for 4 ginkgo saplings in the chamber was ca. 270 ppm/h.

The cultivation condition was as follows: temperature, 26.5–28.5 °C in daytime and 25.0–25.5 °C at night; relative humidity, 75–85 % in the daytime and 55 % in the night; the daytime was from 4:30 to 19:00 in consideration with that in Nagoya. Before the CO_2 administration experiments, the chamber was purged by synthetic air until the $^{12}CO_2$ concentration decreased to <100 ppm. After that, 0.2 L of $^{13}CO_2$ (equal to 600 ppm in the chamber) was supplied every 2 h to adjust the actual CO2 concentration within the 300–1000 ppm range. Finally, the samples were cultivated using plant growth LED lighting for 63 days from 8 June 2018.

The $^{13}CO_2/^{12}CO_2$ ratio of the atmosphere in the chamber was estimated by FT-IR measurements using the FT-720 apparatus (HORIBA, Ltd., Kyoto, Japan). The measurement was conducted using a hand-made gas cell (Fig. S3, internal dimension 20×20×180 mm^3, both sides were sealed by polyethylene films). The calibration curve reported by Wilk et al. (2012) was used to calculate the ratio. The representative FT-IR spectra for the CO_2 region and the resultant $^{13}CO_2/^{12}CO_2$ ratio are shown in Fig. S4 and S5, respectively.

Sampling preparations:

After the cultivation period, the ginkgo samples were harvested, and their leaves were cut off. For microscopic observations and NanoSIMS measurements, a part of the stem was cut as a disk and divided into small blocks (central angle $\pi/4$ and axial length 10 mm) containing bark, cambial zone, and xylem. The small blocks were quickly frozen at −160 °C using liquid Freon®22 (Du Pont) and stored in glutaraldehyde/acetone solution at −80 °C for 3 days, −30 °C for 2 days, 4 °C for 1 day, and then at room temperature.

Other part of the stem was debarked, and the newly formed xylem region was peeled using a peeler as several layers. The thickness of each layer was approximately 0.2 mm. The specimens were extracted by acetone for 8 h using a Soxhlet extractor, extracted by H_2O for 8 h at 80 °C, and freeze-dried. The dried sample was cut by a variable speed rotor mill (PULVERISETTE 14 classic

line, FRITSCH GmbH, Idar-Oberstein, Germany) to obtain a cutting-milled wood (CMW) sample. The CMW sample (1 g) was milled further using a planetary mono mill (PULVERISETTE 6 classic line, FRITSCH GmbH) with zirconia balls (5-mm diameter, 100 g) in a zirconia jar at 600 rpm for 1.5 h (grinding for 2 min, waiting for 2 min, 15 cycles × 3 sets with 20 min intervals) to obtain a ball-milled wood (BMW) sample.

The 1.0-g BMW sample was suspended in 10-mL *N*,*N*-dimethylacetamide at 120 °C for 2 h, dissolved by adding 0.7-g LiCl and stirred overnight at 25 °C. Then, 25 mL of pH 4.8 acetate buffer and 50 mg of meicelase (cellulase originating from *Trichoderma viride*, Meiji Seika Pharma Co. Ltd., Tokyo, Japan) were added to the BMW/DMAc-LiCl solution. The mixture was shaken at 120 rpm, 40 °C for 72 h. During the shaking period, additional 50-mg portions of meicelase were added at 24 h and 48 h after the start of the reaction. The resultant EL samples were washed with H_2O by centrifugation 10 times and freeze-dried. The sample preparation procedure is schematically illustrated in Fig. S1.

Determination of the ^{13}C abundance in the newly formed xylem:

The ^{13}C abundance was evaluated by NanoSIMS and thioacidolysis/GC-MS. The small block sample was embedded in epoxy resin, and a cross-section was prepared using an ultramicrotome (EM-ULTRACUT UCT, Leica, Germany) equipped with a diamond knife. NanoSIMS 50L (Cameca, Gennevilliers, France) measurements were performed using a 16 keV Cs^+ primary ion beam to detect $^{12}C^-$ and $^{13}C^-$ secondary ions. In order to reduce the charging effect, a thin gold layer was deposited on the sample surface. Ion images of 70 × 70 μm^2 were recorded in 256 × 256 pixels. The measured region and the resultant $^{13}C/^{12}C$ ratio visualisations are summarised in Fig. S6.

The CMW samples were applied to thioacidolysis (Nimz 1974; Lapierre et al. 1985, 1991; Rolando et al. 1992). Briefly, 2.5–3.0 mg of the extracted wood sample was placed in 2.5-mL dioxane/ethanethiol mixture (8.75:1, v/v) containing 0.2 M $(C_2H_5)_2OBF_3$ in a test tube. 0.5-mL of 0.5 mg/mL docosane/dioxane solution was added to the tube. Thioacidolysis reaction was run at 100 °C for 4 h and with occasional shaking. Then, 2 mL of 0.4 M $NaHCO_3$ aqueous solution was added to the cooled reaction mixture. The pH of the mixture was adjusted to 2–3 with HCl aqueous solution (1:3 v/v) and extracted with CH_2Cl_2 three times. The combined organic extracts were dried over Na_2SO_4 and evaporated under reduced pressure at 40 °C. The final residue was dissolved in 1.0-mL CH_2Cl_2 for the following GC-MS analysis.

The resultant lignin-derived monomeric products were silylated and injected into GC-MS under the following condition: apparatus, TRACE 1300GC/ITQ 900 (Thermo Fisher Scientific K.K.);

column, Rxi-1 ms (30 m × 0.32 mm I.D., 0.25 μm film thickness); temperature program, 180 °C for 1 min, 180 to 230 °C at 2°C/min, 230 to 300 °C at 15°C/min, and 300 °C for 5 min; column flow, 15.0 mL/min; carrier gas, He; injection temperature, 250 °C. According to the previous report, the monomeric products were evaluated by GC-MS (Lapierre et al., 1991; Roland et al., 1992).

The ^{13}C abundance was calculated using the mass spectrum of guaiacyl unit-derived monomeric product peak. The formula weight of the unit, thioethylated and trimethyl silylated guaiacyl unit (Cα remains), is $[C_8H_7O_2+SC_2H_5+Si(CH_3)_3] = 269$ without isotopes such as ^{13}C. The ^{13}C ratio is calculated using the ion counts from *m*/*z* 269 (none ^{13}C) to 281 (eight ^{13}C in the guaiacyl-derived C_8 unit and other possible +4). The detailed calculation procedure is described in the Supplemental Information and summarised in Fig. S7, Tables S1, S2, S3, S4, and S5.

Solid-state ^{13}C CP and DP/MAS NMR:

Solid-state ^{13}C CP/MAS NMR measurements were conducted on a JEOL ECA-700 spectrometer (JEOL, Ltd., Tokyo). Dried samples under 100-mesh were filled into a 4-mm zirconia sample tube and measured under the following conditions: ^{13}C resonance frequency, 176 MHz; magic angle spinning rate, 14.7 kHz; acquisition time, 29.08 ms. The room temperature was 293 K, and the actual sample temperature in the 14.7 kHz spinning sample tube was estimated as 51.9 °C (r.t. + 31.9 °C) using samarium acetate (Campbell et al. 1986).

The carbon spin-lattice relaxation time (T_1^C) of the EL sample was estimated to determine an adequate relaxation delay for quantitative DP measurements. The pulse sequence proposed by Torchia (1978) was used under the following conditions: contact time, 2 ms; relaxation delay (tau interval), 10 points of 0.1, 0.24, 0.59, 1.44, 3.51, 8.55, 20.80, 50.63, 123.25, and 300.0 s; scan number, 32.

High-speed DP/MAS measurements were carried out using a JEOL ECA-700II spectrometer. Dried samples under 100-mesh were filled into a 1-mm zirconia sample tube and measured under the following conditions: pulse program, "single pulse_dec" by JEOL; ^{13}C resonance frequency, 176 MHz; magic angle spinning rate, 70.0 kHz; acquisition time, 7.26 ms; scan numbers were 512 for CMW, 384 for BMW, and 700 for EL. The pulse program uses 90° pulse. The room temperature was 293 K, and the actual sample temperature in the 70 kHz spinning sample tube was estimated as 63.2 °C (r.t. + 43.2 °C) using $Pb(NO_3)_2$ (Takahashi et al. 1999).

As for solid-state NMR data processing, the obtained FIDs were multiplied with an exponential window function using a line broadening of 20 Hz before the Fourier transform, and phase and baseline corrections were performed using Delta software (v5.0.5.1, JEOL). Finally, the chemical shifts were calibrated using methoxy carbon as an internal standard (56.0 ppm). The T_1^C

relaxation time was obtained using KaleidaGraph (Synergy Software, Inc., Ver. 4.00) from the non-linear least square fit of the signal intensity by the regression formula $y = m_1*\exp(-x/m_2)$ (m_1, initial intensity; m_2, T_1^C). For DP/MAS spectra, Gaussian peak fitting was performed using Excel software (version 2207, Microsoft, US). Three sets of fitting procedures were conducted, and the averaged values were used. Their standard deviations are summarized in Table S8.

Liquid-state ^{13}C NMR:

Liquid-state NMR measurements were conducted with a JEOL ECA-600 spectrometer (^{13}C resonance frequency, 151 MHz). Liquid-state quantitative ^{13}C NMR measurement was carried out using an inverse-gated decoupling mode. The measurement conditions were as follows: pulse program, "single pulse_dec" by JEOL; ^{13}C resonance frequency, 151 MHz; sample concentration, 30 mg/mL; solvent, DMSO-d_6; acquisition time, 1.4 s; relaxation delay, 15 s; scan number 2048; temperature, 295 K. Peak fitting was carried out using Excel software by Gaussian (signals m and n) and Lorentz (other signals) distribution considering their signal broadness.

The T_1^C measurement was performed using the inversion recovery method under the following conditions: scan number, 128; acquisition time, 0.69 s; repetition time, 20.69 s; tau interval, 0.01, 0.03, 0.09, 0.26, 0.77, 2.28, 6.75, and 20.0 s; temperature, 295 K. T_1^C relaxation time was obtained using KaleidaGraph from the non-linear least square fit of the signal intensity by the regression formula $y = m_1*(1-2*\exp(-x/m_2))$. Three sets of fitting procedures were conducted, and the averaged values were used. Their standard deviations are summarized in Table S8.

Results and discussion

Cultivation of *G. biloba* samples in the $^{13}CO_2$ chamber

Samples were successfully cultivated in the airtight growth chamber (Fig. 1) for 63 days. In the growing period, CO_2 concentration was maintained at ca. 300–1000 ppm, and the ^{13}C ratio of CO_2 in the chamber was monitored and illustrated in Fig. 2. The ^{13}C ratio of CO_2 increased up to 87 % after 26 days. After that, the ^{13}C ratio was maintained at ca. 86–88 % in the cultivation period. The ^{13}C ratio could not reach 99% as the same purity of the $^{13}CO_2$ reagent, which should be the respiration and carbon cycle effect in the plants. Before the administration experiments, the saplings were grown under normal air and should have carbon storage to some extent.

In order to evaluate the resultant ^{13}C ratio of the plant cell wall polymers, two methods were applied. The first is NanoSIMS measurements. NanoSIMS can visualise isotope ratios with high spatial and mass resolutions (Lechene et al. 2006; Kojima et al. 2014). NanoSIMS measured the thin

section of the ginkgo sample, and the $^{13}C/(^{13}C+^{12}C)$ % distribution was visualised in the current year xylem region. The measured positions and the colour-scaled NanoSIMS images are shown in Figs. 3 and S6. As visualised, the carbons gradually changed from ^{12}C to ^{13}C, and a high ^{13}C ratio was observed between the cambial zone and the xylem region 400-μm distant from the cambial zone.

Thioacidolysis is a useful analytical method for lignin. Thioacidolysis selectively cleaves the β-*O*-4 linkage in the lignin and can detect the monomeric product derived from the monolignols of guaiacyl (G), syringyl, and *p*-hydroxyphenyl (H) units. In this study, the authors carried out thioacidolysis, and GC-MS analyses of the $^{13}CO_2$ administered ginkgo samples to estimate the ^{13}C ratio in the lignin structural unit. In the gas chromatogram, G-unit derived degradation product was detected, but that from H-unit was not detected.

The G-unit derived monomeric product detected in GC-MS has *m*/*z* 269 as a monoisotopic mass of $[C_8H_7O_2+SC_2H_5+Si(CH_3)_3]$ containing thioethyl and trimethylsilyl groups. Here, if the molecule contains 1–8 of ^{13}C, the *m*/*z* varies from 270–277. Conversely, the actual ^{13}C ratio of the lignin unit can be estimated using the mass variation of the ion. The detailed procedures are described in Supplementary Information. By the calculation, the $^{13}CO_2/(^{13}CO_2+^{12}CO_2)$ % was evaluated for each layer of the peeled samples and summarised in Table 1. The ^{13}C ratio was 88.3–88.8 % within the first to the third layer samples.

These values of ^{13}C ratio evaluated by FT-IR as a carbon source, by NanoSIMS as whole cell wall, and by thioacidolysis/GC-MS as lignin units showed good agreement. The administered $^{13}CO_2$ was converted to plant cell wall polymers. Consequently, the newly-formed xylem regions within the range of 0–400 μm from the cambial zone, the first and the second layer samples, are used for NMR measurements.

T_1^C in solid- and liquid-state ^{13}C NMR

Relaxation time is essential for doing quantitative analyses in NMR (Heitner et al. 2010). In general, 5 times of T_1^C as a relaxation delay for each pulse is needed to recover the signal intensity to 99.33%. In this study, T_1^C measurements were carried out for EL in solid- and liquid-state to do quantitative NMR measurements of the lignin moieties in CMW and BMW in solid-state and EL in solid- and liquid-state. The variations of the signal intensities are illustrated in Fig. S8, and the evaluated T_1^C values are summarised in Tables 2 and S6.

As a result of the EL sample, T_1^C for the signals at 113.1, 120.6, 132.4, and 148.3 ppm were estimated as 7–7.7 s in solid-state; T_1^C for the signals at 111.9, 115.6, 135.5, 147.5 and 150.1 ppm were estimated as 0.4–1.32 s in liquid-state. Previously, T_1^C for dried *Zea mays* sample was reported using solid-state 2D ^{13}C-^{13}C correlation spectra under 10 kHz MAS on the 400-MHz spectrometer

(Kang et al. 2019); the values were 7.3–7.5 s for guaiacyl unit, 6.3–7.3 s for syringyl unit, and 7.3–8.9 s for *p*-hydroxyphenyl unit. For liquid-state NMR, T_1^C for lignin signals was reported 1.52 s in maximum (Landucci 1991). From these results, relaxation delays for solid- and liquid-state were set to 200 s and 15 s, respectively. These values should be long enough to satisfy the quantitative measurement conditions. Additionally, T_2^H and T_2^C values were evaluated for EL in solid- and liquid-state and summarised in Table S6. T_2 values were smaller than the usual coupling constant in 2D NMR measurements (e.g., 8–15 Hz in long-range correlations) and suggest the relatively larger molecular weight of the EL sample as a result of the mild preparation process.

Liquid-state NMR spectrum

Liquid-state quantitative ^{13}C NMR spectrum of EL aromatic region (90–160 ppm) and its signal fitting results are shown in Figs. 4a and S9. Whole region (0–200 ppm) spectra without fittings are displayed in Fig. S10. Signal classifications were based on previous reports for liquid-state NMR (Nimz et al. 1981; Drumond et al. 1989; Xie and Terashima 1991; Hawkes et al. 1993; Robert 1994; Alves et al. 2000; Pårkas et al. 2004; Zhang et al. 2006; Faching et al. 2007; Ralph et al. 2009; Ralph and Landucci 2010; Wen et al. 2013; Li et al. 2016; Yue et al. 2016; Tobimatsu et al. 2019) and for solid-state NMR as described later, and summarised in Tables 3 and S7. Although the EL sample was treated by polysaccharide-degrading enzyme, the signal s derived from residual polysaccharides was still detected due to the incomplete removal. Saccharide signals are also suggested by HSQC spectrum of EL (Fig. S11).

As for lignin aromatic signals, it is impossible to separate all types of lignin structures in the region on 1D spectrum, and most signals are the sum of overlapping signals. For this point, recent NMR studies use 2D NMR techniques to detect and recognise structural differences. However, the quantitative discussion with 2D NMR data is still difficult, although many researchers have proposed new pulse programs and data processing techniques (e.g., Heikkinen et al. 2003; Capanema et al. 2004; Sette et al. 2011, 2013; Yuan et al. 2013; Giraudeau 2014; Tobimatsu et al. 2019). Furthermore, solid-state NMR spectra are generally broader than that in liquid-state.

In this study, the authors aim to evaluate the structural alteration of lignin moieties to surmise the original lignin structures and adopt the following peak-fitting procedure for the NMR data. First, the EL/DMSO spectrum was divided into three areas, as shown in Fig. 4a. Using the genuine software (DELTA by JEOL), the peak areas were evaluated as "by ppm" in Table 4. Then, the NMR spectrum was resolved by peak fitting techniques. Except for the saccharide-derived signal (s), areas of I (a,b,c,d), II (e,f,g,h,i), and III (j,k,l,m,n) were estimated as "by fitting" in Table 4. As a result, these two ways of area integration agreed well. Here, it should be clarified that these resolved signals are

not assigned to the specific lignin aromatic carbon but a base to apply this peak fitting approach to the solid-state NMR spectra.

Solid-state NMR spectra and the peak area alteration

Solid-state ^{13}C DP/MAS NMR spectra of CMW, BMW, and EL aromatic region (90–160 ppm) are displayed in Figure 4 with their signal fitting results. With the high ^{13}C ratio, solid-state quantitative spectra were obtained in reasonable measurement time. As seen in Fig. 4, solid-state NMR spectra (Figs. 4b, 4c, and 4d) were much broader than liquid-state (Fig. 4a). According to the liquid-state NMR spectrum, the peak fitting by Gaussian-type function was performed on the solid-state NMR spectra (Fig. 4b,4c,4d). The grey lines are the original curve, and the plotting lines having circles are the composite curves. Signal classifications were performed considering the previous reports (Hatcher 1987; Hatfield et al. 1987; Xie and Terashima 1991; Hawkes et al. 1993; Wikberg and Maunu 2004; Bardet et al. 2007; Harman-Ware et al. 2017; Evstigneyev et al. 2018; Aoki et al. 2019; Kang et al. 2019) and summarised in Tables 3 and S7.

The most natural-state spectrum of CMW (Fig. 4d) had the sharpest saccharide signal s, and lignin aromatic regions were suppressed. After a ball-milling, the signal s was broadened (BMW, Fig. 4c). Finally, after the enzymatic saccharification, the signal s was smaller than lignin signals (EL, Fig. 4b). About the high-speed MAS contribution (70 kHz), the same samples were also measured in 14.7 kHz MAS and shown in Fig. S9. High-speed MAS is generally effective for samples with ordered structures such as protein. Therefore, its contribution to lignin of amorphous polymer was expected as minor. As a result, however, the signals of saccharides and lignin were sharpened to some extent, and several shoulders and valleys were visualised in the spectra. This difference positively contributed to the peak fitting accuracy, although the resultant peak area ratios were not so different within these two MAS conditions, as suggested in Table S8.

In Table 4, the area ratio of EL in liquid- and solid-state showed slight differences (< 0.7 %). From this result, it is suggested that the quantitative DP/MAS NMR measurement can provide a comparable result with that in quantitative liquid-state NMR measurement, with the help of the peak fitting approach, although each signal in solid-state (Fig. 4b) was much broader than in liquid-state (Fig. 4a). This should be an expected result, but at the same time, the result indicates that liquid-state NMR can provide information of the whole lignin structures in the sample. Therefore, it can be mentioned that the hidden and undetectable insoluble fraction of lignin needs not be supposed much in liquid-state NMR measurements using a dissolved sample after milling. Nevertheless, the effect of the milling step is not negligible.

In order to trace the structural alteration of wood powder samples within the sample

preparation process to obtain a solution, DP/MAS spectra of BMW and CMW were examined. The area ratio in Table 4 shows that their alterations from CMW to EL were 1.1 % on maximum. As a tendency, the area I decreased, and the area II increased. The alteration of area III was the smallest. In the case of 14.7 kHz MAS measurements (Table S8), the tendency of these areas was similar.

In the previous study, ring-5 carbon signals were assigned by the differential spectrum using the [guaiacyl ring-5-^{13}C]-coniferin administered EL sample (Aoki et al. 2019). As described above, in this study, each fitting peak cannot be assigned to the specific carbon; however, the structural alteration can be surmised as a tendency. The area I consists mainly of the aromatic carbons having hydrogen, the area II is derived chiefly from the quaternary aromatic carbons connected to carbon, and the area III can be classified as the quaternary aromatic carbons connected to oxygen. At this point, the alteration tendency, the area I decrement and the area II increment, seems to agree with the formation of condensed-type structures proposed as the milling effect (Ikeda et al. 2002; Fujimoto et al. 2005; Guerra et al. 2006; Hu et al. 2006).

If the area ratio alteration was due only to the ring-5 conditions, the ring-5 carbon alteration could be surmised by the following equations (Eqs. 1–3) based on the assumption that ring-1,2,3,4,6 carbons can be separated into these areas as listed in Table 3. The roughly estimated results are listed in Table 5 and Table S9.

Ring-5 of C-H [Area I %] – 33.33% (2/6 carbons, ring-2 and ring-6) (Eq. 1)

Ring-5 of C-C [Area II %] – 16.67% (1/6 carbons, ring-1) (Eq. 2)

Ring-5 of C-O [Area III %] – 33.33% (2/6 carbons, ring-4 and ring-3) (Eq. 3)

In previous reports, the ring-5 carbon structures were estimated as 48–54 % in uncondensed, 31–39 % in condensed (β-5 and 5-5), and 5–8 % in etherified (4-*O*-5) state for softwood, mainly spruce, by liquid-state NMR (Chen 1996; Capanema et al. 2004; Zhang and Gellerstedt 2007: Sette et al. 2011), and for *G. biloba* xylem with long ball-milling of 6h, the authors reported as 40 % in uncondensed, 45 % in condensed (β-5 and 5-5), and 15 % in etherified (4-*O*-5) state (Aoki et al. 2019). The assumed results in this study may agree with the above results. However, this calculation ignores several possible structures, such as cinnamyl alcohols, cinnamyl aldehydes, spirodienone structures, and some possible degradation products containing double bonds. And it should be mentioned here this area ratio discussion is based on the assumption that any specific lignin moiety was not lost and only the structural alteration is estimated as relative intensity. Further development of peak separation techniques is needed for a better quantitative evaluation of the native lignin structures.

Conclusions

G. biloba saplings were cultivated in $^{13}CO_2$ atmosphere, and high ^{13}C ratio (ca. 85%) wood

meal samples were obtained. After the T_1^C evaluation, quantitative NMR measurements were conducted for CMW, BMW, and EL samples. The aromatic carbon region in ^{13}C NMR spectra was divided into three groups using a peak fitting technique, and the peak area ratio alteration was discussed based on the tentative peak assignments.

The quantification result of EL in liquid- and solid-state agreed well. The result indicates that liquid-state NMR can provide information on the whole lignin structures in the sample as much as solid-state. The peak ratio was not so different between BMW and EL samples. Therefore, the ball-milling effect is dominant in the lignin structural alteration and may cause a relative increase in aromatic C-C compared to aromatic C-H.

Acknowledgements:

The authors thank K. Koga and Y. Maeda, Technical Centre of Nagoya University, and F. Hayashi, RIKEN RSC-Rigaku Collaboration Centre, for helping NMR measurements. This work was supported by JSPS KAKENHI Grant Numbers 15K07510, 18H03959, and 19K06168. NanoSIMS measurements were supported by Nanotechnology Platform project by the Ministry of Education, Culture, Sports, Science and Technology (MEXT), Japan. Solid-state high-speed MAS NMR measurements were performed at Riken Yokohama NMR Facility of NMR Platform (PF19-01-R-025) supported by MEXT, Japan.

Author contributions:

SM, DA, YM, and KF conceived the research. SM and DA cultivated samples and conducted NMR measurements. MT performed NanoSIMS measurements. SM and DA wrote the manuscript. All authors read and contributed to the manuscript.

Conflict of Interest

The authors declare that they have no competing interests.

Supporting Information

Additional Supporting Information may be found in the online version of this article.

Fig. S1 The airtight growth chamber and the sample preparation scheme.

Fig. S2 Temperature and relative humidity transition in the chamber.

Fig. S3 A hand-made gas cell for FT-IR measurements

Fig. S4 The representative FT-IR spectrum of the chamber-atmosphere.

Fig. S5 $^{13}CO_2/^{13}CO_2$ ratio transition in the chamber.

References

Alves, V.L., Drumond, M.G., Stefani, G.M., Chen, C.-L., Piló-Veloso, D. (2000) Synthesis of New Trimeric Lignin Model Compounds Containing 5-5' and β-*O*-4' Substructures, and their Characterisation by 1D and 2D NMR Techniques. *J. Braz. Chem. Soc.* 11:467–473.

Aoki, D., Nomura, K., Hashiura, M., Imamura, Y., Miyata, S., Terashima, N., Matsushita, Y., Nishimura, H., Watanabe, T., Katahira, M., Fukushima, K. (2019) Evaluation of ring-5 structures of guaiacyl lignin in *Ginkgo biloba* L. using solid- and liquid-state ^{13}C NMR difference spectroscopy. *Holzforschung* 73:1083–1092.

Bardet, M., Gerbaud, G., Trân, Q.-K., Hediger, S. (2007) Study of interactions between polyethylene glycol and archaeological wood components by ^{13}C high-resolution solid-state CP-MAS NMR. *J. Archaeol. Sci.* 34: 1670–1676.

Campbell, G.C., Crosby, R.C., Haw, J.F. (1986) ^{13}C Chemical Shifts Which Obey the Curie Law in CP/MAS NMR Spectra. The First CP/MAS Chemical-Shift Thermometer. *J. Magn. Reson.* 69:191–195.

Capanema, E.A., Balakshin, M.Y., Kadla, J.F. (2004) A Comprehensive Approach for Quantitative Lignin Characterisation by NMR Spectroscopy. *J. Agric. Food Chem.* 52:1850–1860.

Chen, C.-L. (1996) Characterisation of milled wood lignins and dehydrogenative polymerisates from

monolignols by carbon-13 NMR spectroscopy. In *ACS Symposium Series 697 Lignin and Lignan Biosynthesis*, Eds. Lewis, N.G., Sarkanen, S. American Chemical Society, Washington, DC, pp. 255–275.

Dimmel, D. (2010) Overview. In: *Lignin and Lignans: Advances in Chemistry*. Eds. Heitner, C., Dimmel, D.R.Schmidt, J.A. CRC Press, Boca Raton. pp. 1–10.

Drumond, M., Aoyama, M., Chen, C.-L., Robert, D. (1989) Substituent effects on C-13 chemical shifts of aromatic carbons in biphenyl type lignin model compounds. *J. Wood Chem. Technol.* 9: 421–441.

Evstigneyev, E.I., Mazur, A.S., Kalugina, A.V., Pranovich, A.V., Vasilyev, A.V. (2018) Solid-State ^{13}C CP/MAS NMR for Alkyl-O-Aryl Bond Determination in Lignin Preparations. *J. Wood Chem. Technol.* 38:137–148.

Fasching, M., Schröder, P., Wollboldt, R.P., Weber, H.K., Sixta, H. (2008) A new and facile method for isolation of lignin from wood based on complete wood dissolution. *Holzforschung* 65:15–23.

Fujimoto, A., Matsumoto, Y., Chang, H. M., Meshitsuka, G. (2005) Quantitative evaluation of milling effects on lignin structure during the isolation process of milled wood lignin. *J. Wood Sci.* 51:89–91.

Giraudeau, P. (2014) Quantitative 2D liquid-state NMR. *Magn. Reson. Chem.* 52:259–272.

Guerra, A., Filpponen, I., Lucia, L.A., Saquing, C., Baumberger, S., Argyropoulos, D.S. (2006) Toward a better understanding of the lignin isolation process from wood. *J. Agric. Food Chem.* 54:5939–5947.

Guittet, E., Lallemand, J.Y., Lapierre, C., Monties, B. (1985) Applicability of the ^{13}C NMR ″INADEQUATE″ experiment to lignin, a natural polymer. Tetrahedron lett. 26:2671–2674.

Hatcher, P.G. (1987) Chemical structural studies of natural lignin by dipolar dephasing solid-state ^{13}C nuclear magnetic resonance. *Org. Geochem.* 11:31–39.

Hatfield, G.G., Maciel, G.E., Erbatur, O., Erbatur, G. (1987) Qualitative and Quantitative Analysis of Solid Lignin Samples by Carbon- 13 Nuclear Magnetic Resonance Spectrometry. *Anal. Chem.* 59:172–179.

Harman-Ware, A.E., Happs, R.M., Davison, B.H., Davis, M.F. (2017) The effect of coumaryl alcohol incorporation on the structure and composition of lignin dehydrogenation polymers. *Biotechnol. Biofuels* 10:281.

Hawkes, G.E., Smith, C.Z., Utley, J.H.P., Vargas, R.R., Viertler, H. (1993) A comparison of solution and solid state ^{13}C NMR spectra of lignins and lignin model compounds. *Holzforschung* 47:302–312.

Heikkinen, S., Toikka, M.M., Karhunen, P.T., Kilpeläinen, I.A. (2003) Quantitative 2D HSQC (Q-

HSQC) via Suppression of *J*-Dependence of Polarization Transfer in NMR Spectroscopy: Application to Wood Lignin. *J. Am. Chem. Soc.* 125:4362–4367.

Hu, Z., Yeh, T.-F., Chang, H., Matsumoto, Y., Kadla, J.F. (2006) Elucidation of the structure of cellulolytic enzyme lignin. *Holzforschung* 60:389–397.

Ikeda, T., Holtman, K., Kadla, J.F., Chang, H.M., Jameel, H. (2002) Studies on the Effect of Ball Milling on Lignin Structure Using a Modified DFRC Method. *J. Agric. Food Chem.* 50:129–135.

Kang, X., Kirui, A., Widanage, M.C.D., Mentink-Vigier, F., Cosgrove, D.J., Wang, T. (2019) Lignin-polysaccharide interactions in plant secondary cell walls revealed by solid-state NMR. *Nat. Commun.* 10:347.

Kojima, T., Yamada, H., Isobe ,M., Yamamoto, T., Takeuchi, M., Aoki, D., Matsushita, Y., Fukushima, K. (2014) Compositional changes of human hair melanin resulting from bleach treatment investigated by nanoscale secondary ion mass spectrometry. *Skin Res. Technol.* 20:416–421.

Landucci, L.L. (1985) Quantitative ^{13}C NMR Characterization of Lignin 1. A methodology for high precision. *Holzforschung* 39:355–359.

Landucci, L.L. (1991) Application of modern liquid-state NMR to lignin characterizasion 2. ^{13}C signal resolution and useful techniques. *Holzforschung* 45:425–432.

Lapierre, C., Monties, B., Rolando, C. (1985) Thioacidolysis of lignin: comparison with acidolysis. *J. Wood. Chem. Technol.* 5:277–292.

Lapierre, C., Pollet, B., Monties, B., Roland, C. (1991) Thioacidolysis of spruce lignin: GC-MS analysis of the main dimers recovered after Raney nickel desulphuration. *Holzforschung* 45:61–68.

Lapierre, C., Pollet, B., Rolando, C. (1995) New insights into the molecular architecture of hardwood lignins by chemical degradative methods. *Res. Chem. Intermed.* 21:397–412.

Lechene, C., Hillion, F., McMahon, G., Benson, D., Kleinfeld ,A.M., Kampf, J.P., Distel, D., Luyten, Y., Bonventre, J., Hentschel, D., Park, K.M., Ito, S., Schwartz, M., Benichou, G., Slodzian, G. (2006) High-resolution quantitative imaging of mammalian and bacterial cells using stable isotope mass spectrometry. *J. Biol.* 5:20.

Lesage, A., Bardet, M., Emsley, L. (1999) Through-Bond Carbon-Carbon Connectivities in Disordered Solids by NMR, *J. Am. Chem. Soc.* 121:10987–10993.

Li, Y., Akiyama, T., Yokoyama, T., Matsumoto, Y. (2016) NMR Assignment for Diaryl Ether Structures (4-O-5) Structures in Pine Wood Lignin. *Biomacromolecules* 17:1921–1929.

Lu, F., Ralph, J. (1997) Derivatisation followed by reductive cleavage (DFRC Method), a new method for lignin analysis: Protocol for Analysis of DFRC Monomers, *J. Agric. Food Chem.* 45:2590–2592.

Lu, F., Ralph, J. (2003) Non-degradative dissolution and acetylation of ball-milled plant cell walls: high-resolution solution-state NMR. *Plant J.* 35:535-544.

Mao, J., Holtman, K.M., Scott, J.T., Kadla, J.F., Schmidt-Rohr, K. (2006) Differences between Lignin in Unprocessed Wood, Milled Wood, Mutant Wood, and Extracted Lignin Detected by ^{13}C Solid-State NMR. *J. Agric. Food Chem.* 54:9677–9686.

Niklas, K.J. Pratt, L.M. (1980) Evidence for Lignin-Like Constituents in Early Silurian (Llandoverian) Plant Fossils. *Science* 209:396–397.

Nimz, H. (1974) Beech Lignin—Proposal of a constitutional scheme. *Angew. Chem. Int. Ed.* 13:313–321.

Nimz, H.H., Robert, D., Faix, O., Nemr, M. (1981) Carbon-13 NMR Spectra of Lignins 8 Structural differences between lignins of hardwoods, softwoods, grasses and compression wood. *Holzforschung* 35:16–26.

Nishimura, H., Kamiya, A., Nagata, T., Katahira, M., Watanabe, T. (2018) Direct evidence for α ether linkage between lignin and carbohydrates in wood cell walls. *Sci. Rep.* 8:6538.

Parkås, J., Paulsson, M., Terashima, N., Westermark, U., Ralph, S. (2004) Light-induced yellowing of selectively ^{13}C-enriched dehydrogenation polymers (DHPs). Part 2. NMR assignments and photoyellowing of aromatic ring 1-, 3-, 4-, and 5-^{13}C DHPs. *Nord. Pulp Paper Res. J.* 19:44–52.

Ralph, J., Akiyama, T., Kim, H., Lu, F., Schatz, P.F., Marita, J.M, Ralph, S.A., Reddy, M.S.S., Chen, F., Dixon, R.A. (2006) Effects of Coumarate 3-Hydroxylase Down-regulation on Lignin Structure, *J. Biol. Chem.* 281:8843–8853.

Ralph, S., Ralph, J., Landucci, L.L. (2009) NMR Database of Lignin and Cell Wall Model Compounds Available from https://www.glbrc.org/databases_and_software/nmrdatabase/ (Sep. 2022 accessed).

Ralph, J., Landucci, L.L. (2010) 5 NMR of Lignins. In *Lignin and Lignans Advances in Chemistry*, Eds. Heitner, C., Dimmel, D.R., Schmidt, J.A. CRC Press, Boca Raton. pp. 137–244.

Ralph, J., Akiyama, T., Coleman, H.D., Mansfield, S.D. (2012) Effects on Lignin Structure of Coumarate 3-Hydroxylase Downregulation in Poplar, *Bioenerg. Res.* 5:1009–1019.

Robert, C. (1994) 5.4 Carbon-13 Nuclear Magnetic Resonance Spectrometry. In: *Methods in Lignin Chemistry*. Eds. Lin, S.Y., Dence, C.W. Springer-Verlag, Berlin, Germany. pp. 250–273.

Rolando, C., Monties, B., Lapierre, C. (1992) Thioacidolysis. In: *Methods in Lignin Chemistry*. Eds. Lin, S.Y., Dence, C.W. Springer-Verlag, Berlin, Germany. pp. 334–349.

Sette, M., Wechselberger, R., Crestini, C. (2011) Elucidation of lignin structure by quantitative 2D NMR. *Chem. Eur. J.* 17:9529–9535.

Sette, M., Lange, H., Crestini, C. (2013) Quantitative HSQC Analyses of Lignin: A Practical

Comparison. *Comput. Struct. Biotechnol. J.* 6: e201306016.

Sipponen, M.H., Laakso, S., Baumberger, S. (2014) Impact of ball milling on maise (*Zea mays* L.) stem structural components and on enzymatic hydrolysis of carbohydrates. *Ind. Crops Prod.* 61:130–136.

Tai, D.-S., Chen, C.L., Gratzl, J.S. (1990) Chemistry of Delignification During Kraft Pulping of Bamboos, *J. Wood Chem. Technol.* 10:75–99.

Takahashi, T., Kawashima, H., Sugisawa, H., Baba, T. (1999) ^{207}Pb chemical shift thermometer at high temperature for magic angle spinning experiments. *Solid State Nuc. Magn. Reson*. 15:119–123.

Terashima, N., Hafrén, J., Westermark, U., VanderHart, D.L. (2002) Nondestructive Analysis of Lignin Structure by NMR Spectroscopy of Specifically ^{13}C-Enriched Lignins Part 1. Solid state study of Ginkgo wood. *Holzforschung* 56:43–50.

Tobimatsu, Y., Takano, T., Umezawa, T., Ralph, J. (2019) Solution-state multidimensional NMR of lignins: Approached and applications. In *Lignin: Biosynthesis, Functions and Economic Significance*, Eds. Lu, F., Yue, F., Nova Science Publishers, Inc., New York, pp. 79–110.

Torchia, D.A. (1978) The Measurement of Proton-Enhanced Carbon-13 T_1 Values by a Method Which Suppresses Artifacts. *J. Magn. Reson.* 30:613–616.

Wen, J.-L., Sun, S.-L., Xue, B.-L., Sun, R.-C. (2013) Recent Advances in Characterisation of Lignin Polymer by Solution-State Nuclear Magnetic Resonance (NMR) Methodology. *Materials* 6:359–391.

Wikberg, H., Maunu, S.L. (2004) Characterisation of thermally modified hard- and softwoods by ^{13}C CPMAS NMR. *Carbohydr. Polym.* 58:461–466.

Wilk, A., Seichter, F., Kim, S.-S., Tütüncü, E., Mizaikoff, B., Vogy, J.A., Wachter, U., Radermacher, P. (2012) *Anal. Bioanal. Chem.* 402:397–404.

Xia, Z., Akim, L.G., Argyropolous, D.S. (2001) Quantitative ^{13}C NMR Analysis of Lignins with Internal Standards. *J. Agric. Food Chem.* 49:3573–3578.

Xie, Y., Terashima, N. (1991) Selective carbon 13-enrichment of side chain carbons of ginkgo lignin traced by carbon 13 nuclear magnetic resonance. *Mokuzai Gakkaishi* 37:935–941.

Yuan, T.-Q., Sun, S.-N., Xu, F., Sun, R.-C. (2011) Characterisation of Lignin Structures and Lignin–Carbohydrate Complex (LCC) Linkages by Quantitative ^{13}C and 2D HSQC NMR Spectroscopy. *J. Agric. Food Chem.* 59:10604–10614.

Yue, F., Lu, F., Ralph, S., Ralph, J. (2016) Identification of 4−O−5-Units in Softwood Lignins via Definitive Lignin Models and NMR. *Biomacromolecules* 17:1909–1920.

Zhang, L., Gellerstedt, G., Ralph, J., Lu, F. (2006) NMR Studies on the Occurrence of Spirodienone

Structures in Lignins. *J. Wood Chem. Technol.* 26:65–79.

Zhang, L. Gellerstedt, G. (2007) Quantitative 2D HSQC NMR determination of polymer structures by selecting suitable internal standard references. *Magn. Reson. Chem*. 45:37–45.

TABLES and FIGURES

Table 1 $^{13}C/(^{13}C+^{12}C)$ Ratio Evaluated by Thioacidolysis/GC-MS.

Distance from the cambial zone (μm)	$^{13}C/(^{12}C+^{13}C)$ (%)
0–200	89.3
200–400	88.8
400–600	88.3
600–800	9.3
800–1000	4.8

Table 2 Spin-Lattice Relaxation Time T_1^C of EL Aromatic Carbons.

T_1^C (s) solid-state EL (ppm)	T_1^C (s) liquid-state EL in DMSO (ppm)
6.97 (113.1)	0.44 (111.9)
7.20 (120.6)	0.37 (115.6)
7.31 (132.4)	1.21 (135.5)
7.72 (148.3)	1.28 (147.5)
	1.32 (150.1)

Table 3 Peak classifications of aromatic carbons in solid- and liquid-state NMR.

Area	Label	Classification of major carbons	Aromatic carbon assignments in Refs						Fitting peak top (ppm)			
									Solid			Liquid
			1	2	3	4	5	6	CMW	BMW	EL	EL
	s	Saccharides, G2		■					104.5	102.4	104.5	103.3
I	a	G5(-H), G2, G6		■			■	■	109.0	109.8	110.3	111.5
	b			■			■	■	115.9	115.5	116.0	115.4
	c							■	121.9	121.7	121.3	119.4
	d		■					■	122.9	122.1	124.1	123.1
II	e	G5(-C) in β-5,5-5, G1	■				■	■	125.8	126.0	126.0	126.6
	f		■				■		128.9	128.8	128.3	129.2
	g		■				■		132.5	132.5	131.7	132.6
	h		■				■		136.7	136.7	135.9	135.4
	i		■			■			140.0	140.5	140.1	137.9
III	j	G5(-O) in 4-*O*-5, G3, G4	■			■			143.0	143.4	143.3	143.7
	k		■		■	■	■		146.7	146.8	146.8	147.3
	l				■	■			150.4	150.3	150.3	149.7
	m				■	■	■		153.2	152.3	153.0	152.2
	n				■	■			153.3	154.2	155.9	154.0

Table 4 Area ratio (%) of aromatic regions.

	Solid-state (by fitting)			Liquid-state EL	
Area	CMW	BMW	EL	by fitting	by ppm
I	43.3	42.2	42.2	42.0	42.0
II	22.2	23.1	23.0	23.7	23.3
III	34.5	34.7	34.9	34.3	34.7

Table 5 Assumed conditions (%) of ring-5 carbon in lignin estimated by Eqs. 1–3.

	Solid-state			Liquid-state EL	
Ring-5	CMW	BMW	EL	by fitting	by ppm
C-H	60	53	53	52	52
C-C	33	39	38	42	40
C-O	7	8	9	6	8

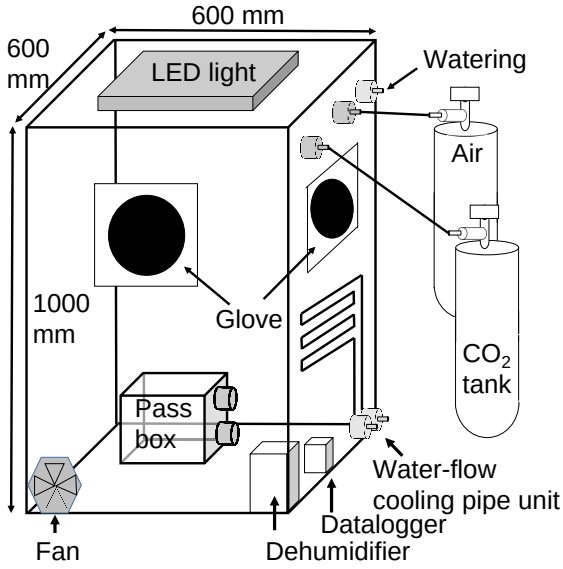

Fig. 1 An overview of the airtight growth chamber.

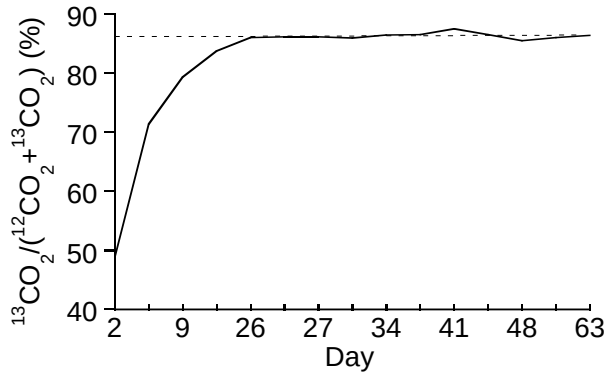

Fig. 2 ^{13}C ratio of the CO_2 in the chamber during the $^{13}CO_2$ administration period.

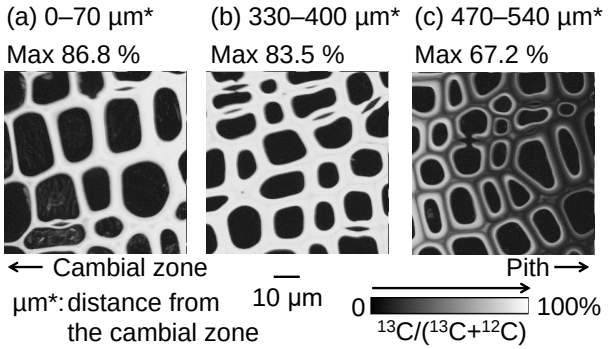

Fig. 3 NanoSIMS results of the $^{13}CO_2$ administered ginkgo wood sample.

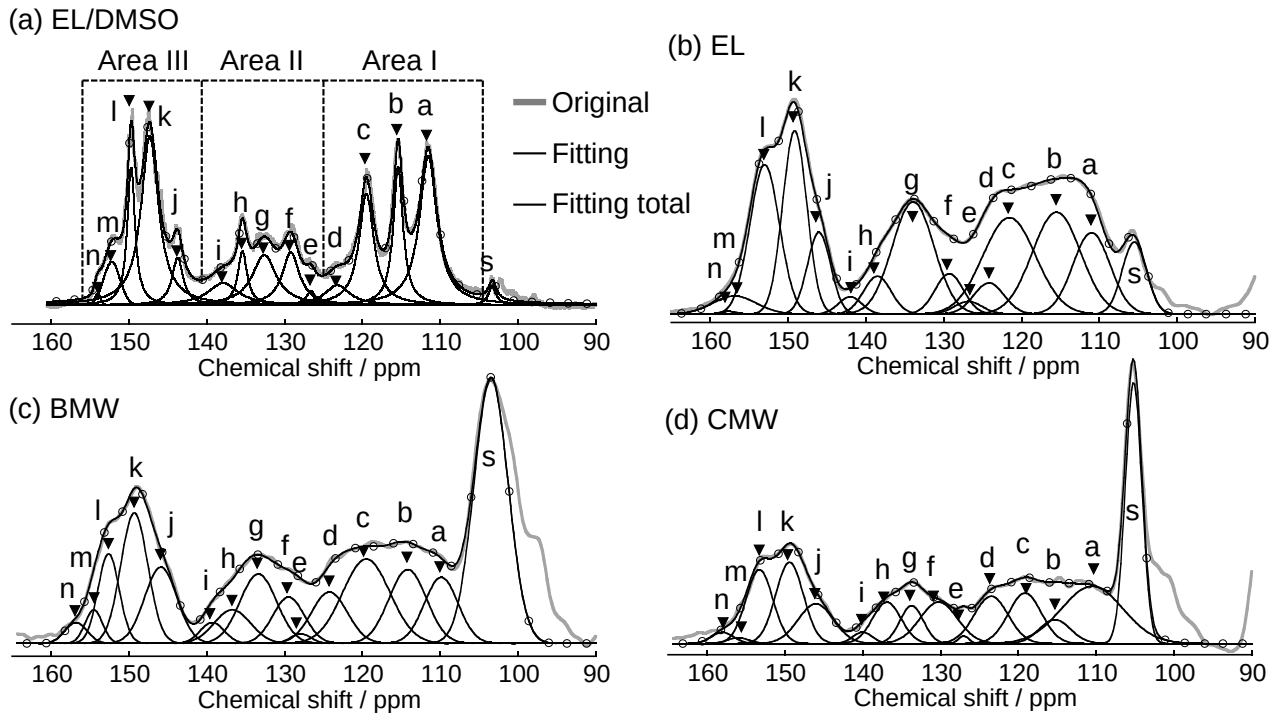

Fig. 4 Quantitative ^{13}C NMR spectra of (a) EL in liquid-state, (b) EL in solid-state, (c) BMW in solid-state, and (d) CMW in solid-state. Peaks (s, a, b, c, d, e, f, g, h, i, j, k, l, m, and n) correspond to the signals in Table 3.

Supporting Information

Evaluation of guaiacyl lignin aromatic structures using $^{13}CO_2$ administered *Ginkgo biloba* L. xylem by quantitative solid- and liquid-state ^{13}C NMR

Sonoka MIYATA[1], Dan AOKI[1*], Yasuyuki MATSUSHITA[2], Miyuki TAKEUCHI[3], Kazuhiko FUKUSHIMA[1]

[1] Graduate School of Bioagricultural Sciences, Nagoya University, Nagoya 464-8601, Japan
[2] Institute of Agriculture, Tokyo University of Agriculture and Technology, Tokyo 183-8509, Japan
[3] Graduate School of Agricultural and Life Sciences, The University of Tokyo, Tokyo 113-8657, Japan
* Corresponding author: aoki.dan@nagoya-u.jp

Contents

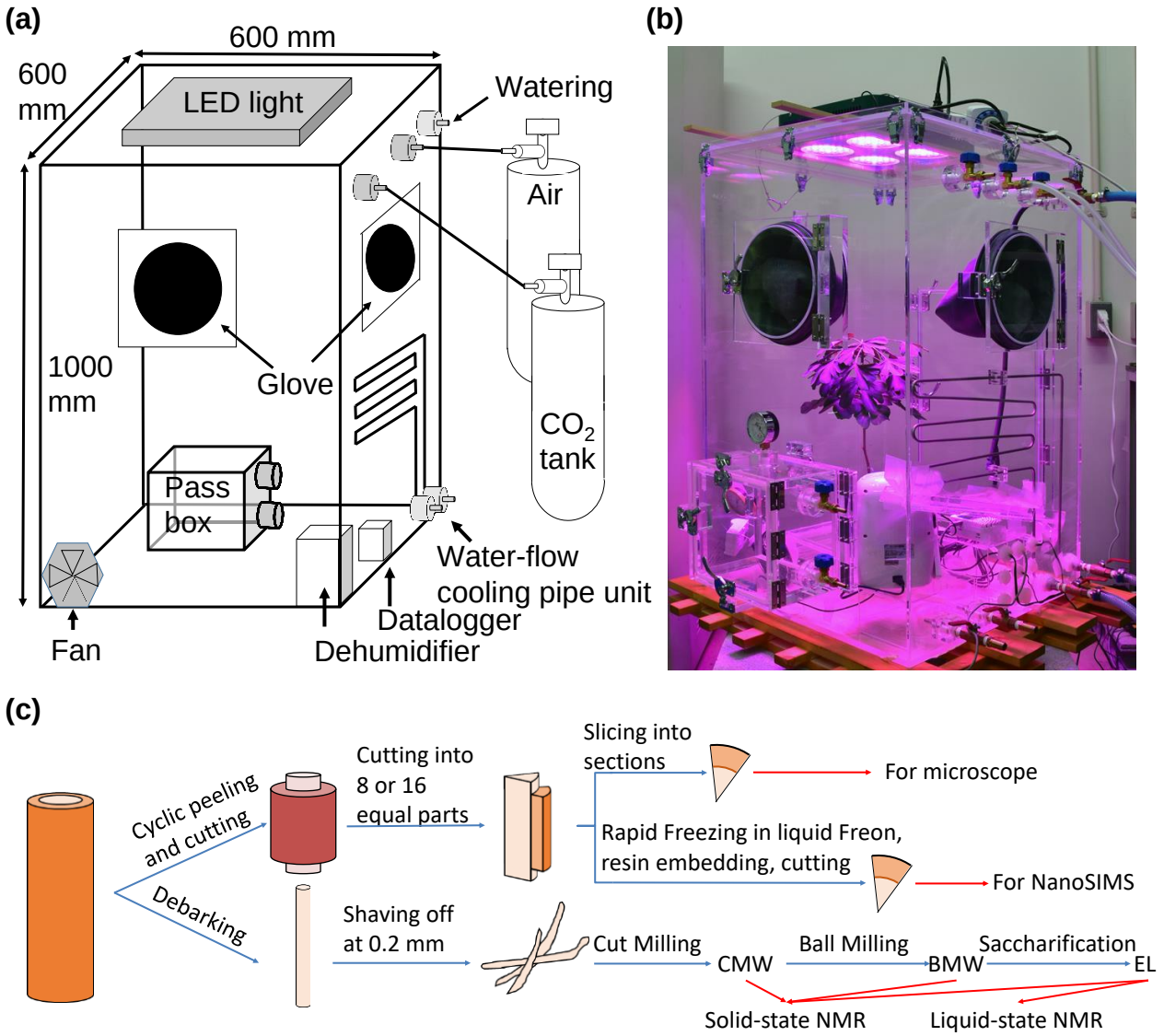

Fig. S1 (a) An overview and (b) a photograph of the airtight growth chamber. (c) Sample preparation procedures.

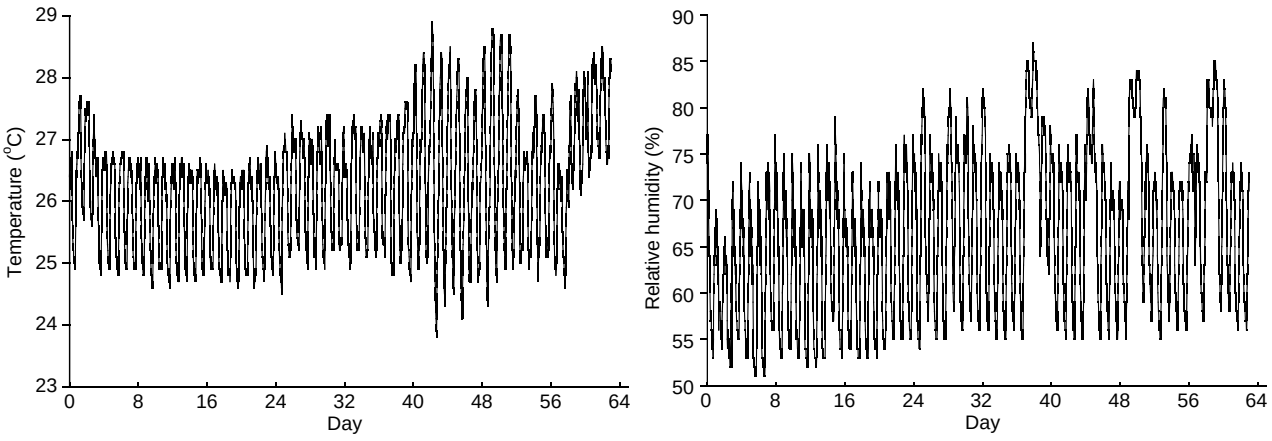

Fig. S2 Temperature and relative humidity transition in the chamber.

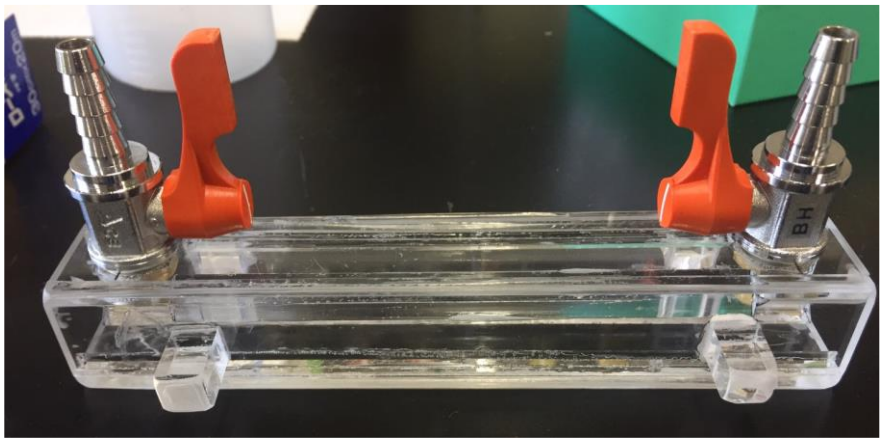

Fig. S3 A **h**and-made gas cell for FT-IR measurements.

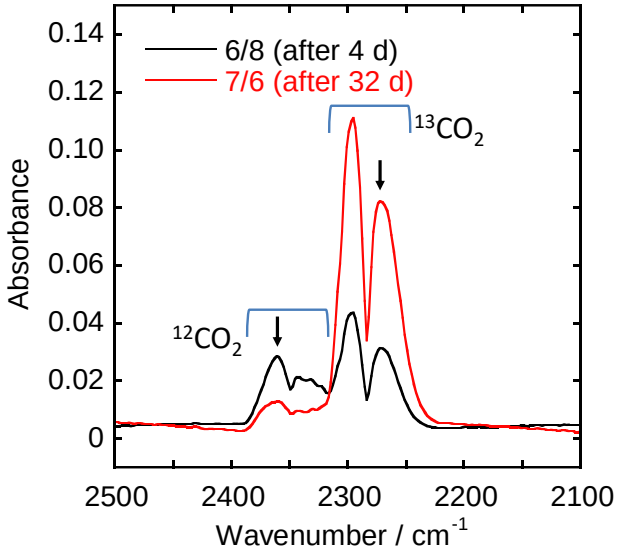

Fig. S4 The representative FT-IR spectra of the chamber-atmosphere. Arrows are the wavenumbers used for the calculation.

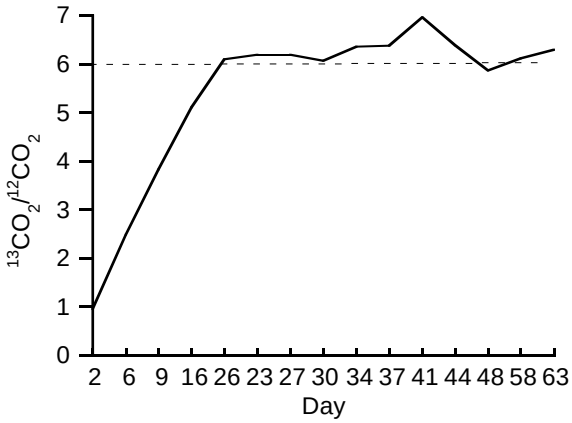

Fig. S5 $^{13}CO_2/^{13}CO_2$ ratio transition in the chamber.

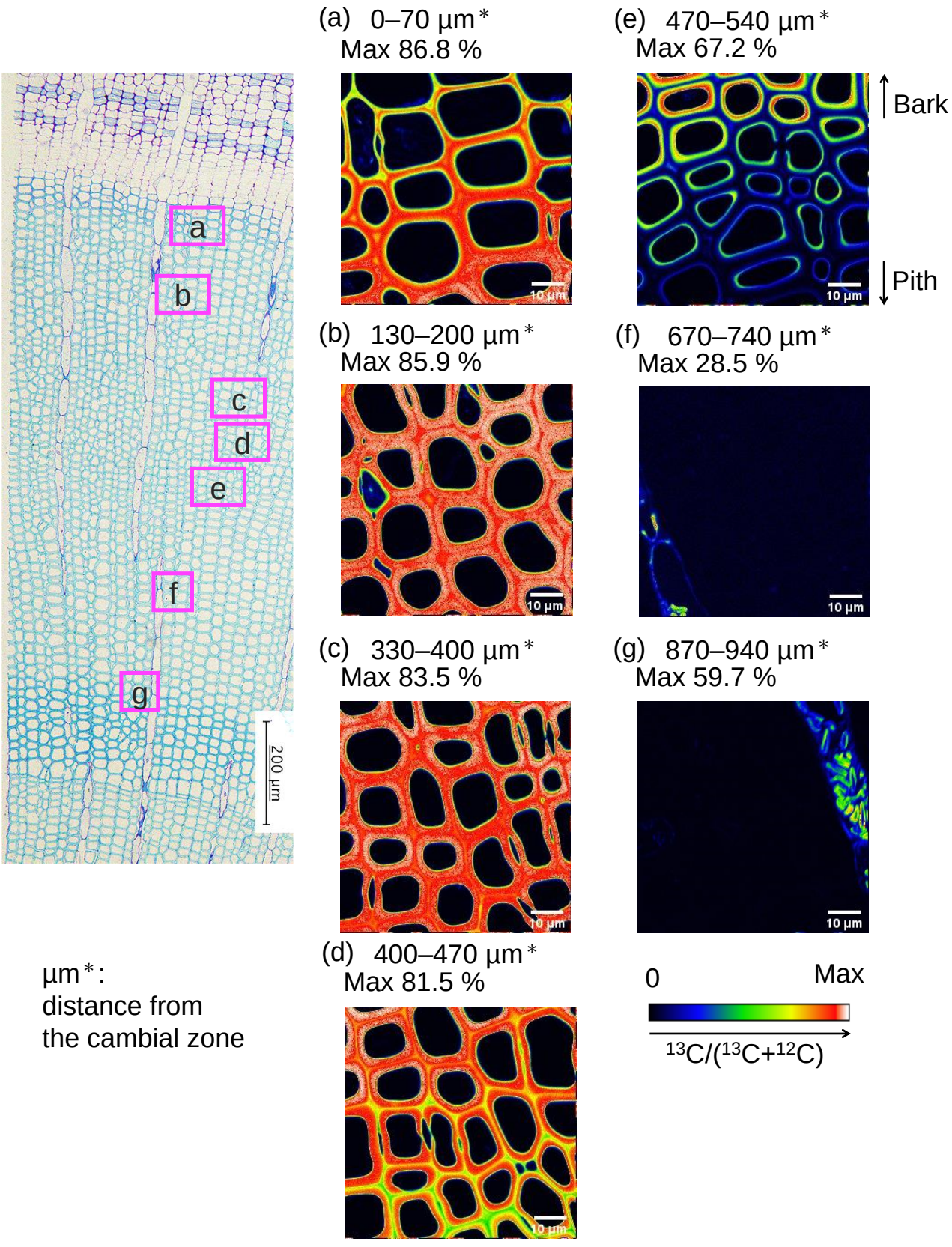

Fig. S6 NanoSIMS results of the $^{13}CO_2$ administered ginkgo wood sample.

Calculation. Estimation of ^{13}C ratio by thioacidolysis/GC-MS.

The concept of estimating the ^{13}C ratio of lignin-derived guaiacyl (G)-unit (Fig. S4) is the least-square calculation of the probability distribution of the *m*/*z* values of the unit.

$C8H7O2 + SC2H5+Si(CH3)3$ (C8+5, H21, O2, Si1, S1)

Here, we suppose that only the ^{13}C ratio of the C8H7O2 group is unknown, and the other isotopic abundance is in the natural state. Thus, we can estimate the variance by simulation of the isotopic mass variation of the unit and fitting calculation with a variance of the lignin-derived 13C ratio.

The following isotope abundances (NIST, Atomic Weights and Isotopic Compositions for All Elements) were used for the calculation.

^{12}C, 0.98938; ^{13}C, 0.01078

^{1}H, 0.999886; ^{2}H, 0.000116

^{16}O, 0.997572; ^{17}O, 0.000381; ^{18}O, 0.002051

^{28}Si, 0.922232; ^{29}Si, 0.046858; ^{30}Si, 0.030921

^{32}S, 0.949926l; ^{33}S, 0.00752; ^{34}S, 0.042524; ^{35}S, 0.00011

Here, ^{2}H and ^{35}S are quite a low abundance and omitted in the following calculations.

Next, the mass variation of the lignin-derived G-unit (H21O2Si1S1 without C) can be expressed as follows:

$$(^{1}H)^{21}(A^{16}O + A^{17}O + A^{18}O)^{2}(A^{28}Si + A^{29}Si + A^{30}Si)(A^{32}S + A^{33}S + A^{34}S) = 113–121$$

Here, **A** means the abundance and the above equation, and all isotopic patterns are listed and summarized in Table S1 and S2, respectively. As a result of Table S2, the probability of *m*/*z* >118 is quite low and omitted in the following calculations.

Similarly, the ^{13}C ratio of thioethyl and trimethylsilyl units of C5 is calculated and summarized in Table S3, and the cases of *m*/*z* > 113 are omitted.

Finally, using the above values and the variance of the lignin-derived ^{13}C ratio of the C8 unit, the actual *m*/*z* variation of the sample (Table S4) was fitted by Microsoft Excel 2016 Solver function to lead the variance (Table S5). Here, if the all eight of G-unit carbons were ^{13}C and other elements are the smallest isotopes, the ion is *m*/*z* 277. In Table S4, the largest relative abundance was obtained for the *m*/*z* 277 ion in cases of the 1st, 2nd, and 3rd layer samples.

The results suggesting a higher ^{13}C ratio (> 80%) up to the 3rd layers (ca. 600 μm in thickness) agreed with the NanoSIMS results in Fig. S3. Furthermore, the estimated ^{13}C ratio of CO_2 in the chamber (Fig. 1 and S5). Although the cell wall layer-specific differences cannot be evaluated, and this fitting calculation is only possible with the assumption that the ^{13}C distribution is homogeneous in the sample, this 13C ratio calculation by thioacidolysis/GC-MS might be helpful.

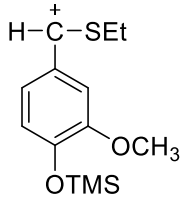

Fig. S7 The chemical structure of the lignin-derived G-unit ($C_{13}H_{21}O_2SiS$).

Table S1 Existence probability of $H_{21}O_2SiS$.

O	Si	S	probability	*m*/*z*	O	Si	S	probability	*m*/*z*
$^{16}O^{16}O$	^{28}Si	^{32}S	0.871802416	113	$^{16}O^{18}O$	^{28}Si	^{32}S	0.00359	115
		^{33}S	0.006901542	114	$^{18}O^{16}O$		^{33}S	2.80E-05	116
		^{34}S	0.039026752	115			^{34}S	0.00016	117
	^{29}Si	^{32}S	0.044295711	114		^{29}Si	^{32}S	0.00018	116
		^{33}S	0.000350663	115			^{33}S	1.40E-06	117
		^{34}S	0.001982924	116			^{34}S	8.20E-06	118
	^{30}Si	^{32}S	0.029230272	115		^{30}Si	^{32}S	0.00012	117
		^{33}S	0.000231399	116			^{33}S	9.50E-07	118
		^{34}S	0.00130851	117			^{34}S	5.40E-06	119
$^{16}O^{17}O$	^{28}Si	^{32}S	0.000665931	114	$^{17}O^{18}O$	^{28}Si	^{32}S	1.40E-06	116
$^{17}O^{16}O$		^{33}S	5.27E-06	115	$^{18}O^{17}O$		^{33}S	1.10E-08	117
		^{34}S	2.98E-05	116			^{34}S	6.10E-08	118
	^{29}Si	^{32}S	3.38E-05	115		^{29}Si	^{32}S	7.00E-08	117
		^{33}S	2.68E-07	116			^{33}S	5.50E-10	118
		^{34}S	8.16E-06	117			^{34}S	3.10E-09	119
	^{30}Si	^{32}S	2.23E-05	116		^{30}Si	^{32}S	4.60E-08	118
		^{33}S	1.77E-07	117			^{33}S	3.60E-10	119
		^{34}S	1.00E-06	118			^{34}S	2.10E-09	120
$^{17}O^{17}O$	^{28}Si	^{32}S	1.27E-07	115	$^{18}O^{18}O$	^{28}Si	^{32}S	3.70E-06	117
		^{33}S	1.01E-09	116			^{33}S	2.90E-08	118
		^{34}S	5.69E-09	117			^{34}S	1.70E-07	119
	^{29}Si	^{32}S	6.46E-09	116		^{29}Si	^{32}S	1.90E-07	118
		^{33}S	5.12E-11	117			^{33}S	1.50E-09	119
		^{34}S	2.89E-10	118			^{34}S	8.40E-09	120
	^{30}Si	^{32}S	4.26E-09	117		^{30}Si	^{32}S	1.20E-07	119
		^{33}S	3.38E-11	118			^{33}S	9.80E-10	120
		^{34}S	1.91E-10	119			^{34}S	5.50E-09	121

Table S2 Existence probability of $H_{21}O_2SiS$ as a sum.

m/z	probability
113	0.871802
114	0.051863
115	0.072232
116	0.002477
117	0.001599
118	1.04E-05
119	5.68E-06
120	1.14E-08
121	5.53E-09
Sum	1

Table S3 Existence probability of C_5.

^{13}C numbers	*m/z*	probability
0	60	0.94725
1	61	0.051613
2	62	0.001125
3	63	1.23E-05
4	64	6.68E-08
5	65	1.46E-10
	Sum	1

Table S4 The *m*/*z* variation of G-unit derived ions as a thioacidolysis monomeric products.

m/z	1st (%)	2nd (%)	3rd (%)	4th (%)	5th (%)
269	1.07	0.89	13.93	28.28	44.98
270	1.78	2.00	4.83	8.92	10.27
271	5.63	5.77	6.32	7.90	7.93
272	1.96	2.19	2.73	2.75	2.81
273	1.93	2.38	2.93	2.93	2.03
274	4.00	4.27	4.67	3.88	3.05
275	10.70	11.73	10.34	8.09	5.44
276	28.28	27.22	21.90	14.89	9.56
277	35.17	34.01	25.34	16.79	9.98
278	5.62	6.11	4.18	2.74	1.95
279	3.18	2.98	2.20	1.74	0.97
280	0.43	0.35	0.40	0.35	0.48
281	0.26	0.11	0.23	0.73	0.53
Sum	100	100	100	100	100

Table S5 Calculated ^{13}C ratio of $^{13}CO_2$ administered ginkgo samples.

Sample layers	$^{13}C/ (^{12}C+^{13}C)$ (%)
1st	89.27
2nd	88.83
3rd	86.30
4th	9.28
5th	4.78

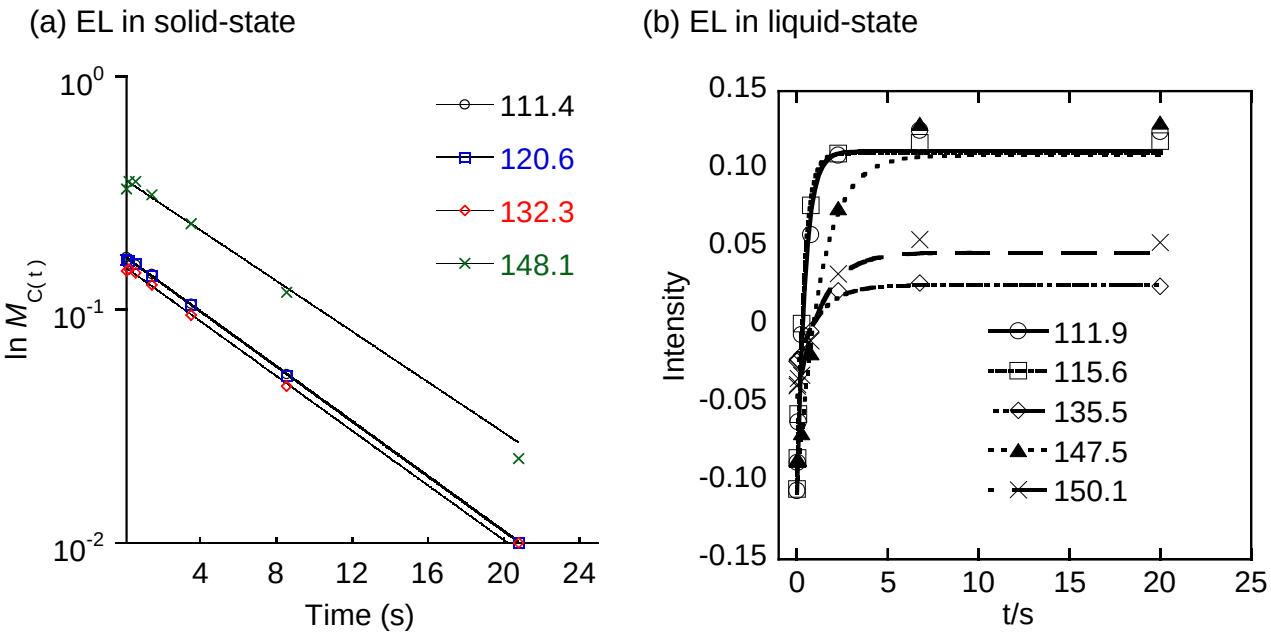

Fig. S8 Signal intensity depending on the relaxation delay of EL in (a) solid-state and (b) liquid-state NMR to evaluate T_1^C values.

Table S6 T_1^H, T_1^C, T_2^H, and T_2^C values for the EL sample.

Solid-state EL	Liquid-state EL	
T_1^C/s (ppm)	T_1^H/s (ppm)	T_1^C/s (ppm)
7.58 (56.0)	1.02 (3.6)	0.84 (56.0)
6.80 (62.7)	1.09 (4.7)	0.22 (60.6)
6.81 (74.8)	1.08 (5.0)	0.10 (63.6)
6.34 (82.6)	1.10 (5.1)	0.44 (72.0)
6.97 (113.1)	1.10 (5.3)	0.44 (73.4)
7.20 (120.6)	1.09 (5.6)	0.38 (75.3)
7.31 (132.4)	1.08 (7.0)	0.50 (84.3)
7.72 (148.3)	1.07 (7.4)	**0.44 (111.9)**
	0.50 (7.7)	0.55 (112.4)
		0.37 (115.6)
		0.35 (119.5)
		1.17 (129.1)
		1.21 (135.5)
		1.28 (147.5)
		1.32 (150.1)
T_2^C/ms (ppm)	T_2^H/ms (ppm)	T_2^C/ms (ppm)
1.49 (56.0)	20.29 (3.6)	41.00 (56.0)
1.01 (62.6)	19.81 (4.6)	14.83 (60.6)
0.88 (74.8)	18.79 (5.0)	14.02 (63.4)
0.92 (82.6)	14.95 (5.4)	13.60 (71.2)
0.99 (105.0)	14.97 (7.0)	12.20 (72.0)
0.75 (113.6)		14.83 (75.2)
0.77 (120.3)		12.36 (84.2)
1.12 (132.4)		10.50 (111.8)
1.59 (147.9)		8.85 (112.1)
		14.89 (115.5)
		15.96 (119.4)
		7.15 (129.8)
		7.27 (135.9)
		39.92 (147.9)
		41.45 (150.0)

* Bold values are listed in Table 2.

For T_2 evaluation, protocols of "t2_cpmas.ex2" and "cpmg_dec.ex2" made by JEOL were used for solid-state and liquid-state measurements, respectively.

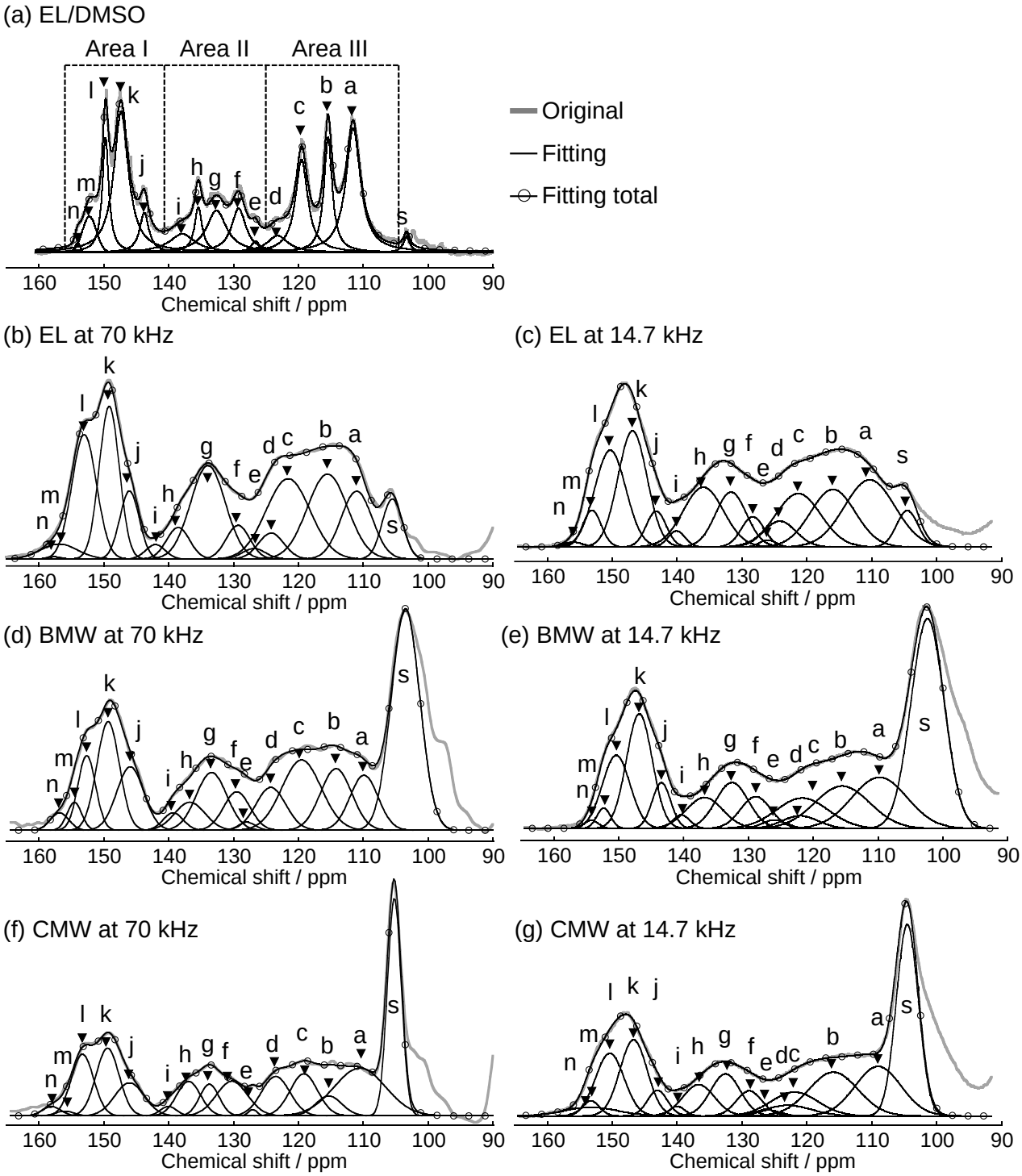

Fig. S9 Quantitative ^{13}C NMR spectra of (a,b,c) EL, (c, d) BMW, and (f,g) CMW samples. Samples were measured with (a) ^{13}C inverse-gated decoupling mode and (b,c,d,e,f,g) ^{13}C DP/MAS mode. MAS rates for solid-state NMR were (b,d,f) 70.0 kHz and (c,e,g) 14.7 kHz.

Quantitative DP/MAS measurements at 14.7 kHz were conducted using JEOL ECA-700 spectrometer (JEOL, Ltd., Tokyo). Dried samples under 100-mesh were filled into a 4-mm zirconia sample tube and measured under the following conditions: relaxation delay, 200 s and scan number, 256.

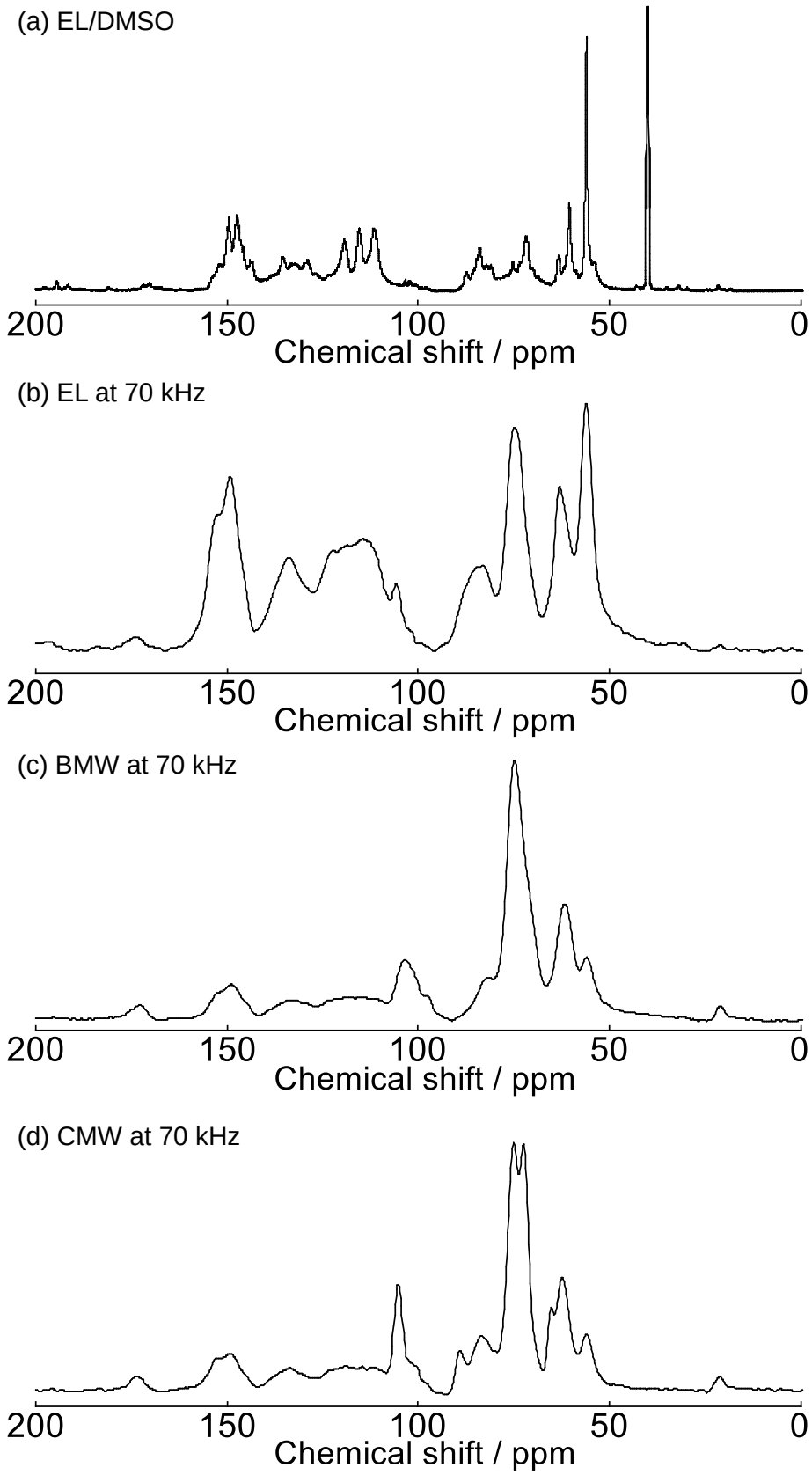

Fig. S10 Quantitative ^{13}C NMR spectra without fittings of (a,b) EL, © BMW, and (d) CMW samples.

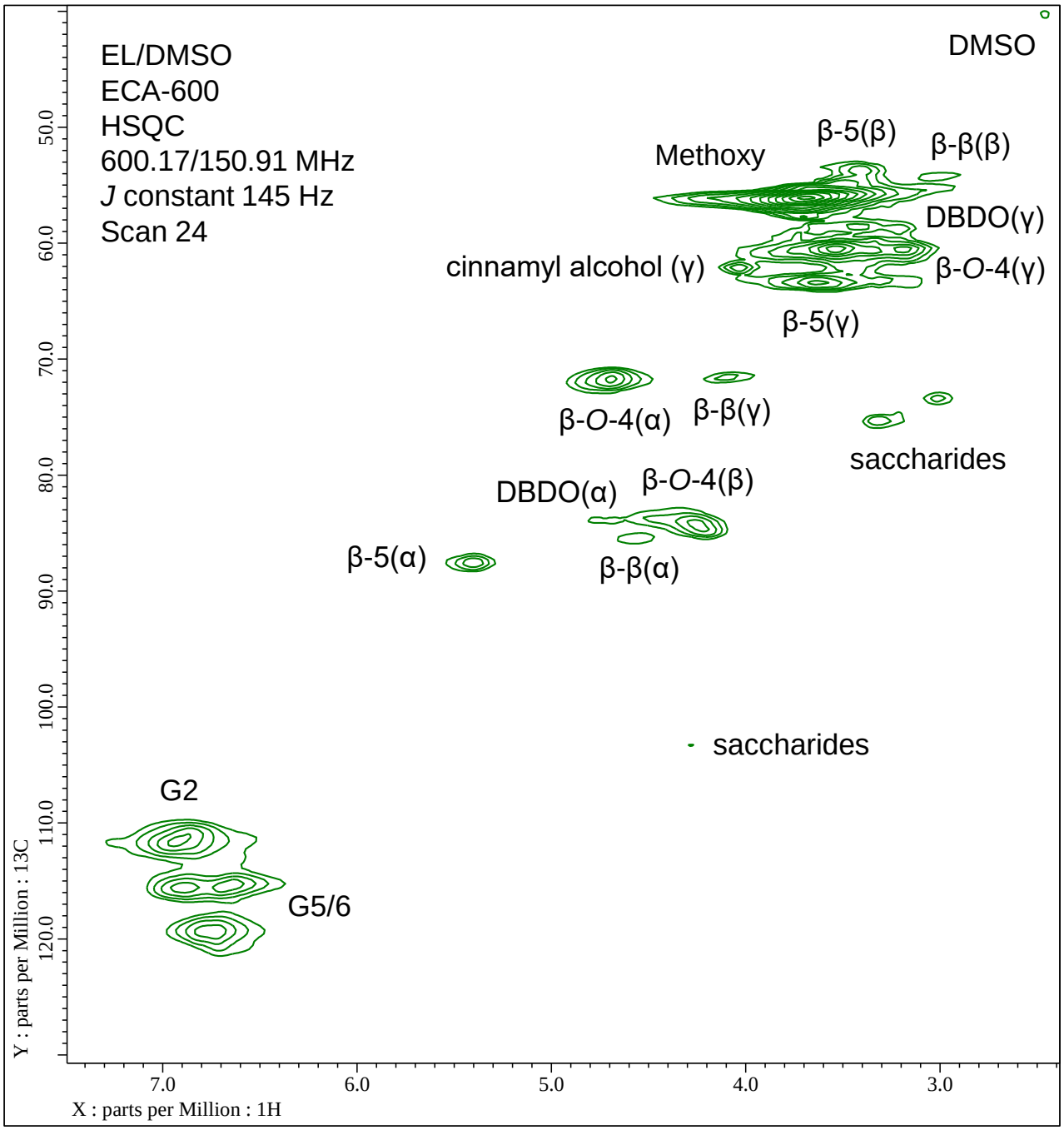

Fig. S11 HSQC spectrum of EL in DMSO-d_6. Measured by JEOL ECA-600 spectrometer. Text suggests the C-H position in the linkage type; for example, β-*O*-4(α) means the Cα-H cross signal in the β-*O*-4 linkage. DBDO means dibenzodioxocin. G2, G5/G6 means the aromatic ring-2, ring-5/ring-6 carbons in the lignin guaiacyl units.

Table S7 Peak classifications of aromatic carbons in solid- and liquid-state NMR.

		Major	Carbon positions						Solid			Assignments in References								
		carbons	1	2	3	4	5	6	CMW	BMW	EL	1	2	3	4	5	6	7	8	9
	s	Sac., G2							104.5	102.4	104.5		Sac.				2	2		
I	a	G5(-H), G2, G6							109.0	109.8	110.3	5	5,6	2,5	2	2	5	2,5	2	
	b								115.9	115.5	116.0	5	5,6	2,5	5	5	5	2,5	5	
	c								121.9	121.7	121.3		6					6	6	
	d								122.9	122.1	124.1		6				6	1,6		
II	e	G5(-C) in β-5, 5-5, G1							125.8	126.0	126.0	5		1,5		6	6	1,5		
	f								128.9	128.8	128.3			1,5				1		1,5
	g								132.5	132.5	131.7	5	1	1	1				1	1
	h								136.7	136.7	135.9		1	1	1,5	1	1			
	i								140.0	140.5	140.1			1			1			1,4
III	j	G5(-O) in 4-O-5, G3, G4							143.0	143.4	143.3				4			3,4		
	k								146.7	146.8	146.8	5	1,4	3,4	3,4	4	4		3,4	
	l								150.4	150.3	150.3			3,4				3,4		3,4
	m								153.2	152.3	153.0	5			3,4			4		3,4
	n								153.3	154.2	155.9						3	4		3,4

		Major	Carbon positions						Liquid	Assignments in References										
		carbons	1	2	3	4	5	6	EL	7	9	10	11	12	13	14	15	16	17
	s	Sac., G2							103.3					Sac.		2		2	2
I	a	G5(-H), G2, G6							111.5	2,5		2	2	2		2	2	6	6
	b								115.4				5	5	5	5	5		
	c								119.4	6		6	6	6		6	6		
	d								123.1			6	1,6				1,6		
II	e	G5(-C) in β-5,5-5, G1							126.6			5	5		1,5		5		
	f								129.2	1			1,6		1,5				
	g								132.6	1	1	1,5	5	1	1,5	5	1,5	1	1
	h								135.4	1	1		1	1	1	1	1		
	i								137.9			1			1		4	4	4
III	j	G5(-O) in 4-O-5, G3, G4							143.7		4	4	4		3,4	4	4	5	
	k								147.3	3,4	4	3	3,4		3,4	3,4	5		
	l								149.7	3,4	3,4		3	3	3	3,4	3	3	5
	m								152.2	4	4	3	5		3				
	n								154.0		4				3	3			3

Table S7 references are referred in main text.

1. Aoki et al. 2019
2. Bardet et al. 2007
3. Evstigeneyev et al. 2018
4. Harman-Ware et al. 2017
5. Hatcher 1987
6. Hatfield et al. 1987
7. Hawkes et al. 1993
8. Kang et al. 2019
9. Xie and Terashima 1991
10. Alves et al. 2000
11. Drumond et al. 1989
12. Nimz et al. 1981
13. Parkås et al. 2004
14. Robert 1994
15. Wen et al. 2013
16. Li et al. 2016
17. Yue et al. 2016

Table S8 Area ratio (%) of aromatic regions.

	Solid-state (by fitting)			Liquid-state	
Area	CMW	BMW	EL	EL	
		70.0 kHz		by fitting	by ppm
I	43.3 (0.07)	42.2 (0.03)	42.2 (0.05)	42.0 (0.07)	42.0 (0.18)
II	22.4 (0.13)	23.1 (0.02)	23.0 (0.02)	23.7 (0.18)	23.3 (0.20)
III	34.5 (0.11)	34.7 (0.01)	34.9 (0.06)	34.3 (0.16)	34.7 (0.12)
		14.7 kHz			
I	42.3 (0.08)	41.2 (0.11)	41.3 (0.14)		
II	22.1 (0.02)	22.7 (0.29)	23.2 (0.07)		
III	35.7 (0.08)	36.1 (0.33)	35.5 (0.22)		

Values in parentheses are standard deviations by three sets of fitting results.

Table S9 Assumed conditions (%) of ring-5 carbon in lignin estimated by Eqs. 1–3.

	Solid-state			Liquid-state	
Ring-5	CMW	BMW	EL	EL	
		70.0 kHz		by fitting	by ppm
C-H	60	53	53	52	52
C-C	33	39	38	42	40
C-O	7	8	9	6	8
		14.7 kHz			
C-H	54	47	48		
C-C	33	36	39		
C-O	14	16	13		

References

NIST, Atomic Weights and Isotopic Compositions for All Elements https://physics.nist.gov/cgi-bin/Compositions/stand_alone.pl?ele=&all=all&ascii=html&isotype=some (Accessed 21st, Aug, 2022)